PAUL SCHERRER INSTITUT

Optics Beamline X05DA– Beamline Handbook

$Author : flechsig$
$Revision : 1.29$
$Date : 2008/04/3006 : 57 : 12$

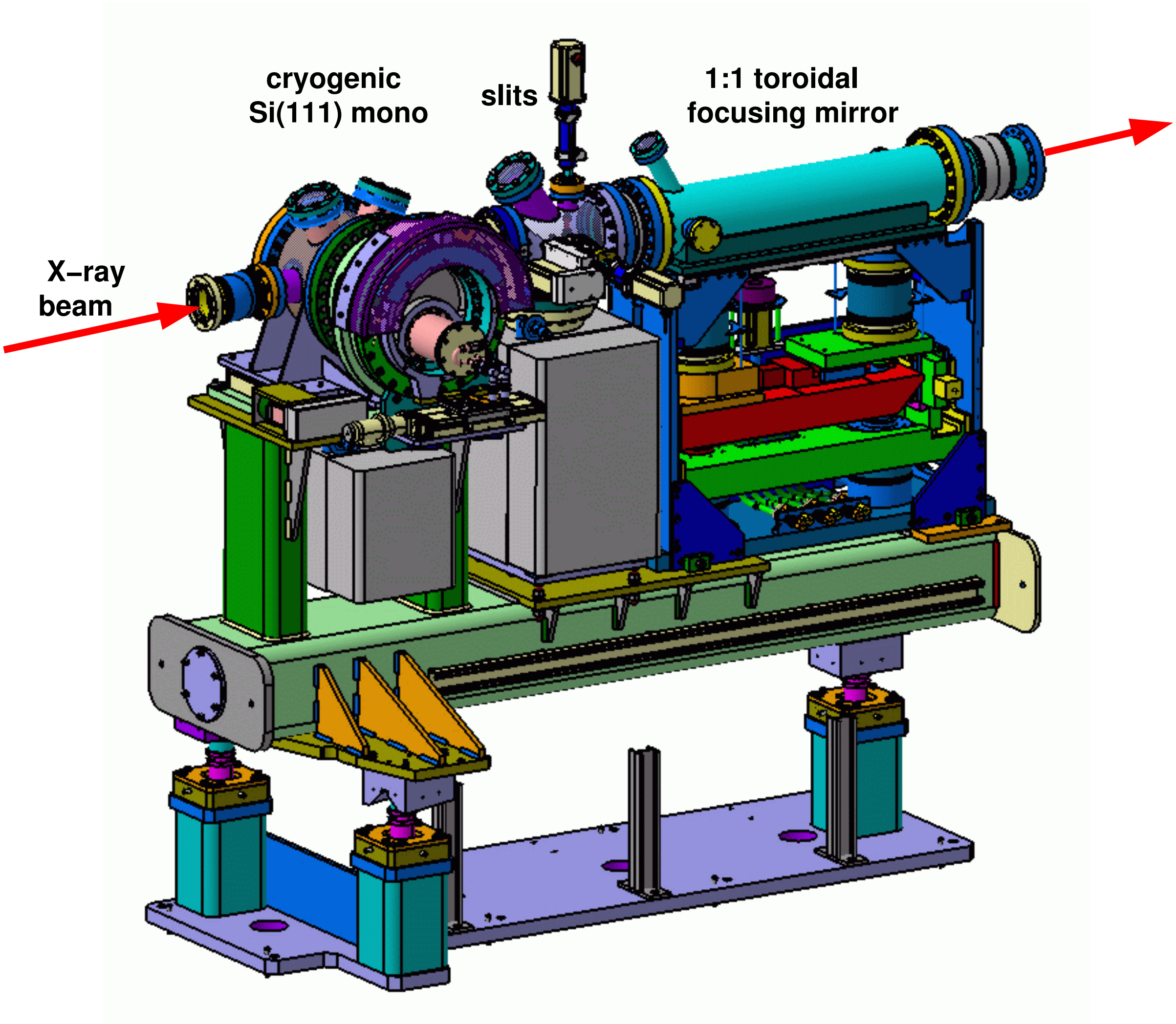

The monochromator and mirror assembly.

About the document

This document is considered as a reference for the SLS Optics Beamline X05DA. The current document concentrates on performance calculations and commissioning measurements which can be of interest for users of the beamline. To trace back how the current solution has been evolved see section 8 and the previous concept study Optics Beamline X05DA from 2004. The LaTeXsource of the document is under cvs control (see version information from cvs tags). There is a common source for the printout (postscript), pdf, and html. The document has been optimized for pdf, the html version (generated with `latex2html`) may lack some features. Some of the hypertext links will not work outside the PSI network due to access restrictions.

Contents

List of Figures

1 Introduction

In 2006 a multipurpose beamline for general experiments in the field of X-ray optics and synchrotron radiation instrumentation has been installed at the SLS dipole magnet X05DA. The beamline shares the experimental hutch with the diagnostics beamline for the SLS machine (X05DB). The beamline covers a photon energy range from 5.5 to 22keV with a cryogenically cooled[1] Si(111) channel cut monochromator and 1 to 1 focusing with a toroidal mirror. Monochromator and mirror can be individually retracted to allow focused/unfocused dipole radiation and unfocused monochromatic beam in addition.

The very compact monochromator- mirror assembly has been installed in the front end area inside the shielding tunnel (Fig. 1). The basic concept is similar to the beamline 11.3.1 at ALS. The beamline has been designed in collaboration with ALS and summarized by Flechsig *et al.* [1] (SRI 2006 poster). The ALS beamline is subject of the following publications by Padmore *et al.* [2] and Thompson *et al.*[3].

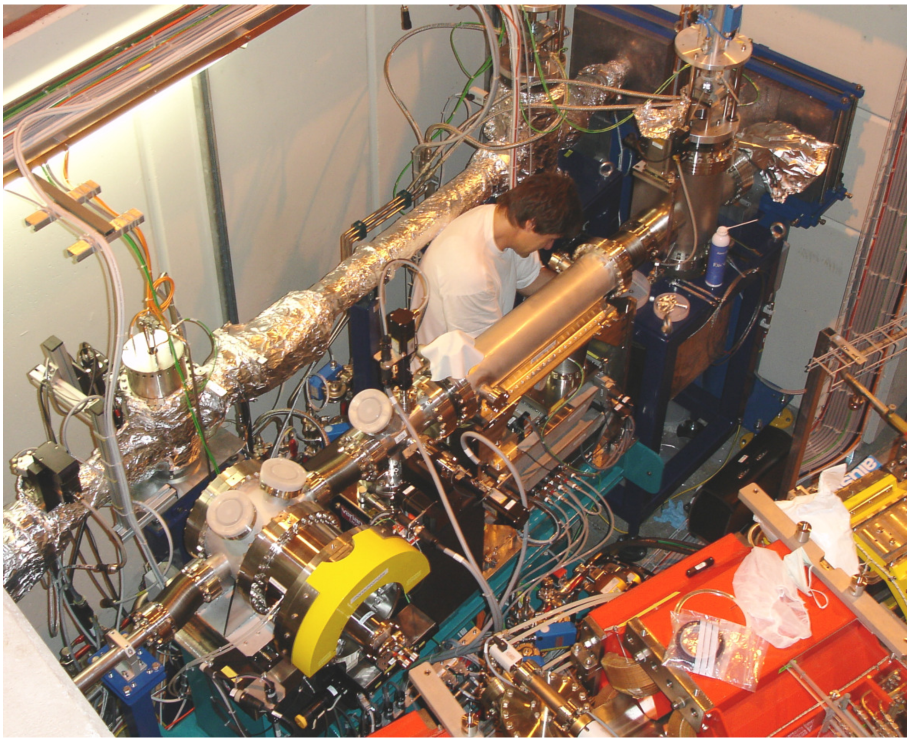

Figure 1: The monochromator- mirror assembly after installation inside the tunnel of the SLS storage ring.

2 Beamline Layout

The optical beamline layout is shown on Fig. 2. We use the downstream part of the central dipole (the SLS uses a triple bent achromat lattice). There is a diaphragm at 5 m (15.5×3) mm or (2.5×0.6) mrad. A $100\,\mu$m thick CVD diamond window (18×6) mm separates the storage ring vacuum (UHV $\approx 10^{-10}$ mbar) from the high vacuum (HV) of the monochromator ($\approx 10^{-8}$ mbar). The window works as a safety element and withstands air pressure[2] A water cooled horizontal slit system is located at 6 m to restrict the horizontal acceptance and the heat load on the crystal.

[1]The thermal expansion coefficient of silicon is zero at 125 K (-148 °C)
[2]Similar windows have been tested up to 4 bar.

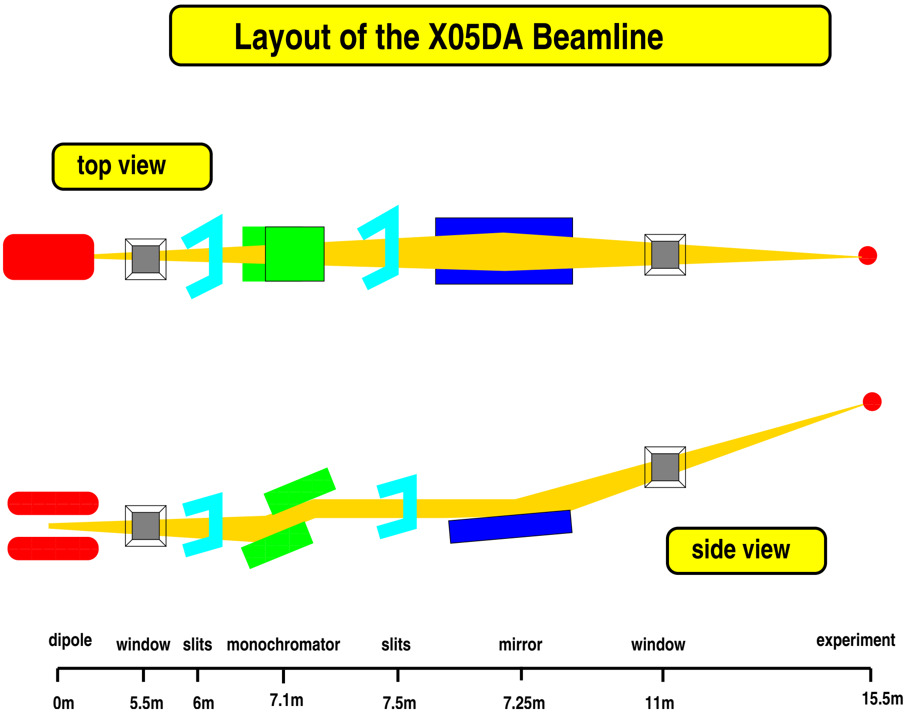

Figure 2: Beamline layout.

The cryogenically cooled Si(111) channel crystal is located at about 7.1 m. The cut width is $w = 3$ mm, reflection upward, the vertical offset of the beams $dy = 2w * \cos\theta$ is about 6 mm. The calculation is shown in Fig 3. The downstream surface has an asymmetry of 0.3° to compress the beam size (see drawing and picture). The cooling is done with a CryoTiger– a closed system with a cold head which is in thermal contact to the crystal via a copper bar, a silicon base plate and an indium foil. The cooling capacity is about 25 W at 120 K.

In front of the crystal there is a water cooled vertical aperture of $(20h \times 2v)$ mm. The monochromator chamber can be retracted horizontally to allow direct dipole radiation.

Downstream the monochromator there is an aperture system with 2 brackets to limit the horizontal beam size. The manipulators are stacked i.e. one defines the position and the other one the width. In the vertical direction there is a manipulator with fixed slits of (3, 2, 1, 0.5) mm width. **The apertures are not water cooled – be careful – do not overheat them!**

The mirror unit has motorized pitch, yaw, height and radius adjustments whereas the vacuum chamber position is fixed. The toroidal shape of the focusing mirror is produced by bending a cylinder (radius 31 mm, size: 400×20 mm, grazing angle 4 mrad, coating: Cr plus 30 nm Pt with 5 nm Rh on top of it). See drawing and image. The mirror is water cooled based on bath cooling with a InGa eutectic. In front of the mirror there is also a fixed water cooled aperture. The mirror together with the aperture can be vertically retracted.

After the shielding wall there is a second 110 μm thick diamond window at the end of the HV section. The window can be vertically moved to comply the beam heights in the different operation modes. It follows an about 5 m long pipe with a rough vacuum (≈ 1 mbar). The beamline ends with a kapton foil.

X05DA does not have beam position monitors- we have to use the monitors from X05DB.

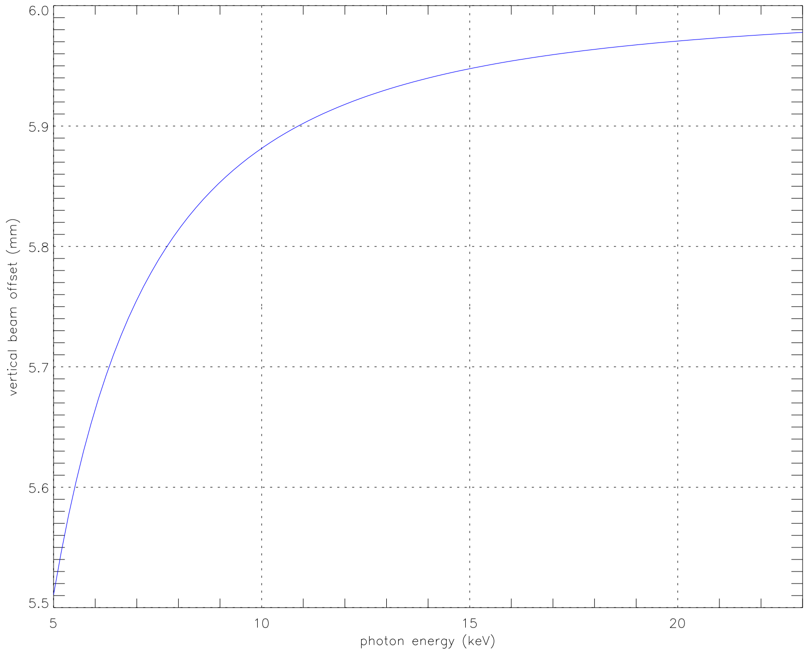

Figure 3: Vertical beam offset in the monochromator as function of the photon energy.

3 Experimental Environment

The experiment has to share the hutch with the machine diagnostics beamline X05DB which was installed before we started to plan X05DA. If one beamline needs access to the hutch the other beamline must interrupt its operation[3]. The last valve of the front end is at 11 m, the max. beam path in the hutch is 10 m, i.e. maximum path length is 21 m. The maximum space for the experiment (4×3) m. The door to the hutch is very small- access for big equipment has to go through the roof.

The experimental infrastructure is under development. We may provide an optical table 2.4 m x 1.5 m (Fig. 4). The table can be moved by air pads. The height can be remotely controlled with an accuracy of $1\,\mu\mathrm{m}$ between 750 and 1050 mm. We will have some motorized stages which can be mounted at X95 profiles. Four analog video cameras can be connected to a video server. A remote controlled network camera is mounted in the hutch. GPIB devices can be connected to a LAN-GPIB bridge.

Experimental equipment foreseen to use at the beamline should be compatible with the VME and EPICS environment.

We provide a patch panel 5 with:

- 9 230V dc outlets
- 1 230V dc outlet, switchable from the control system (for a lamp etc.).
- 8 network sockets
- 16 BNC sockets, to be patched in the rack outside

[3] The machine diagnostics beamline will be used in particular during machine development shift where no stable beam for users is provided. So the direct interference during operation is expected to be small. There is the drawback that we may not have access to the experiment for maintenance and installation during machine shifts.

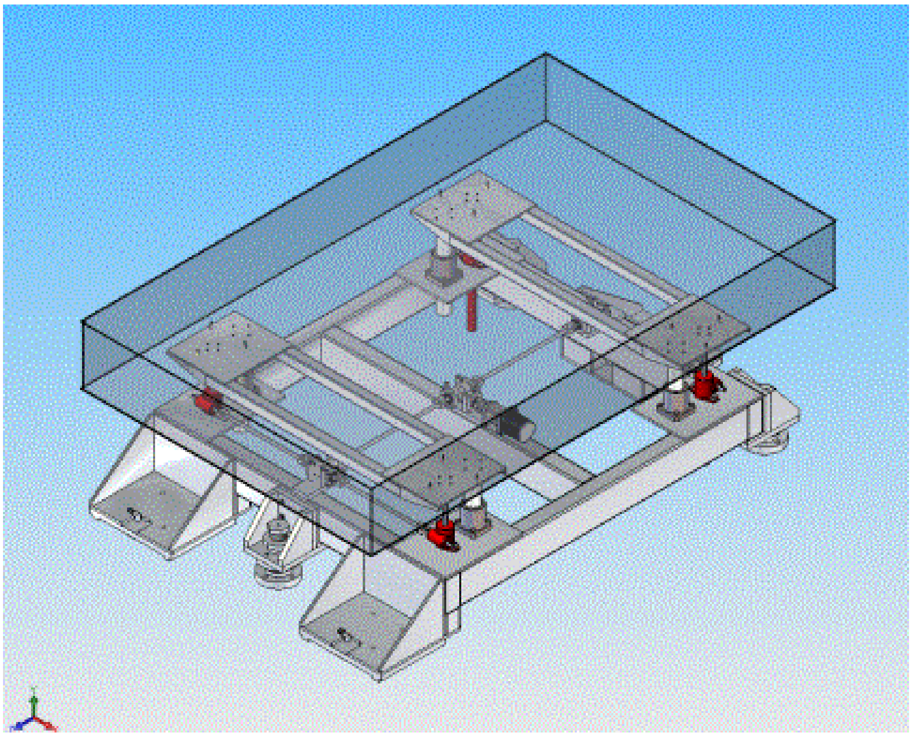

Figure 4: Sketch of the experimental table.

- 8 SHV sockets, to be patched in the rack outside
- 8 sockets for thermoelements
- 16 encoders
- 16 5-phase motors (M1...M16)
- 16 4-phase motors (M17...M32 where M17 is reserved for the optical table).

The cables go to a rack outside which is located beyond the controls hutch. The rack houses the motor amplifiers, the BNC and SHV patch panel and the VME crate with, analog in and out ($\pm 10\,V$, 16 bit, max. 50 kHz), digital in and out. **The current settings of the motor driver has to be checked and adjusted respectively before your own motors can be hooked up!** The default setting for 5-phase motors is 0.75A, 1/20 step (microstepping). The default setting for 4-phase motors is 1.5A, 1/2 step (microstepping). **Be careful and do not mix up 4-phase and 5-phase motors, the drivers and/ or motors may be demaged!** Any change at the motor amplifieres[4] has to be documented at the list which is in the end station- rack. The individual motor parameters and positions can be saved and restored with the provided tools. It is not allowed to change the defaults in the substitution files!

The beamline has a control room of $4\,\mathrm{m} \times 3\,\mathrm{m}$ equipped with a 4-head beamline console `x05da-cons-1`and a color printer `WSLA_X05DA`.

[4] change of current, voltage, microstepping, replacement of drivers etc..

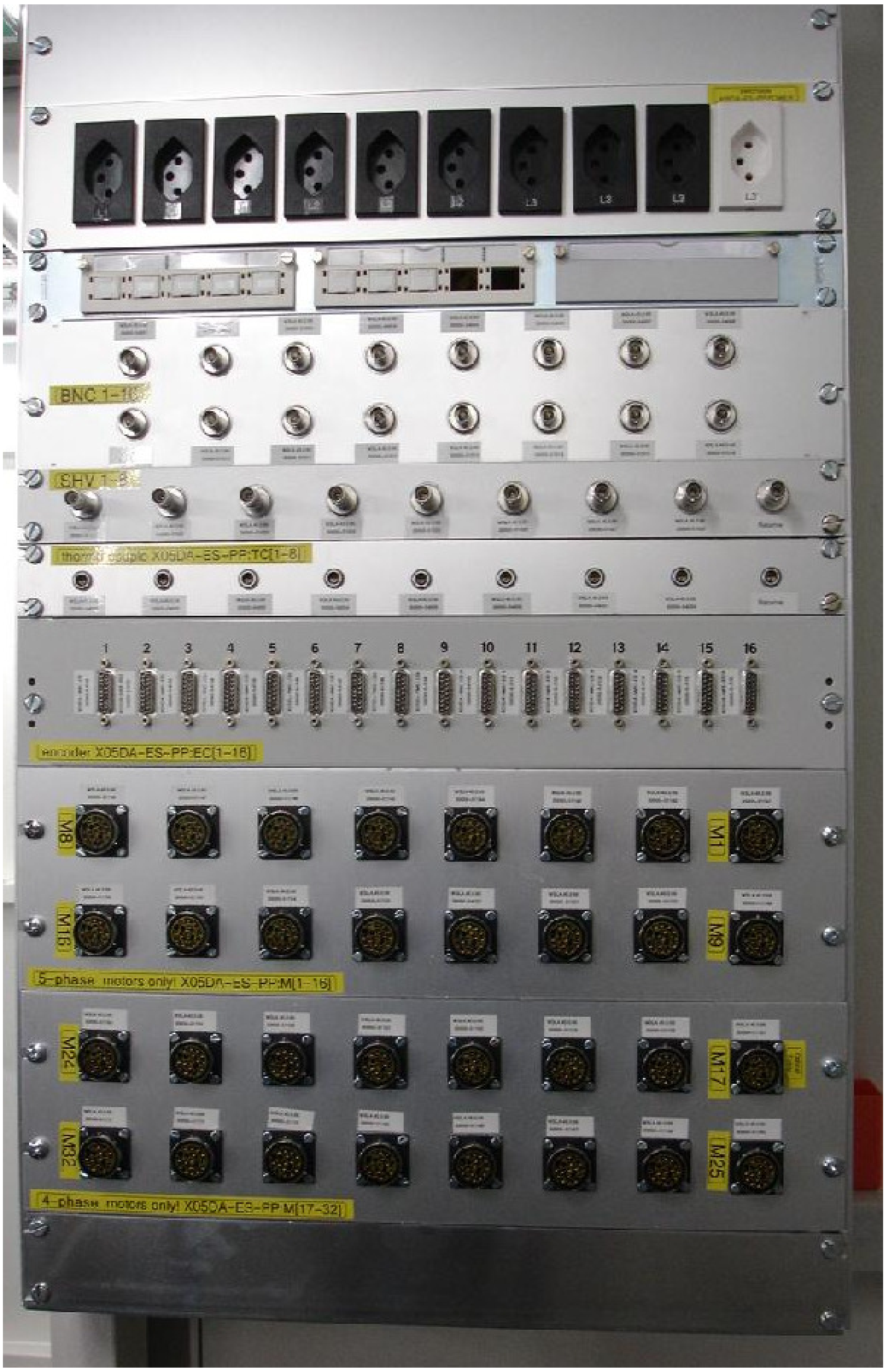

Figure 5: Patch panel inside the X05DA optics hutch.

4 Dipole magnet and monochromator theory

4.1 SLS Dipole

- critical energy: 5.36 keV, $B = 1.4\,\mathrm{T}$, bending radius 5.729 m,
- total integrated power: 32.7 W/mrad (0.4 A ring current, 2.4 GeV).
- on axis power density: 101 W/mrad^2 (0.4 A ring current, 2.4 GeV).
- the flux densities are shown on Fig. 6.
- electron beam size: $(45 \times 23)\mu\mathrm{m}$ $(h \times v)$.

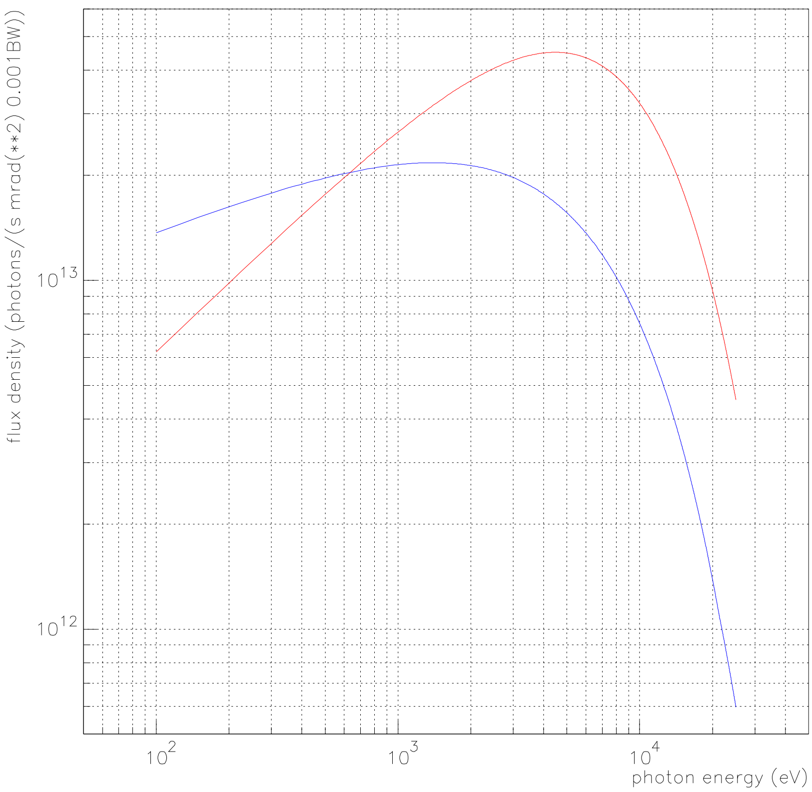

Figure 6: SLS dipole normalized flux densities, ring current 400 mA. Red: on axis flux density in $\mathrm{photons}/(\mathrm{s\ mrad}^2\ 0.001\ \mathrm{BW})$, blue: vertically integrated distribution in $\mathrm{photons}/(\mathrm{s\ mrad}\ 0.001\ \mathrm{BW})$.

The normalized vertical flux density profile for a few selected photon energies is shown on Fig. 7. The extracted FWHM values are shown on Fig. 8.

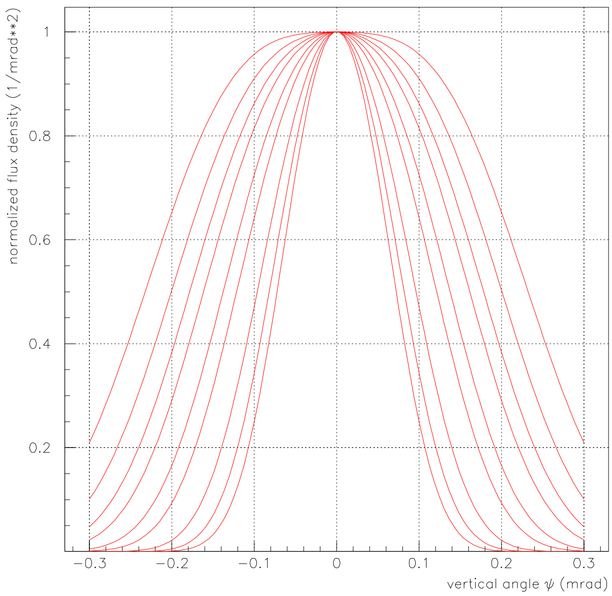

Figure 7: Normalized vertical flux density profile. Photon energy $E = (3,\ 4,\ 5,\ 6,\ 8,\ 10,\ 15,\ 20,\ 25)$ keV (from wide to narrow).

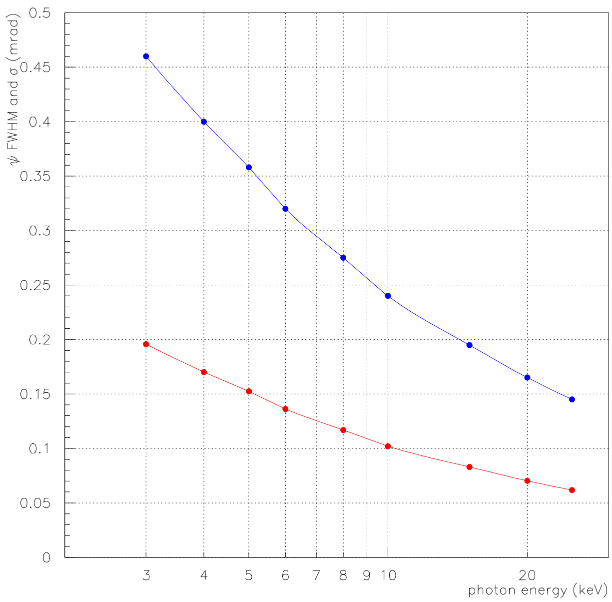

Figure 8: Vertical flux density FWHM (blue) and σ (red).

4.2 General bending magnet theory

The critical energy ϵ_c is the energy where 50% of the vertical integrated power is below that energy and above respectively. In case of the SLS dipole: $\epsilon_c = 5.36$ keV, 16 W/mrad are below ϵ_c and 16 W/mrad above.

The photon flux density on axis (vertical observation angle $\psi = 0$) in practical units $[\mathrm{photons}/(\mathrm{s\ mrad}^2\ 0.001\ \mathrm{BW})]$ is

$$\left.\frac{d^2F}{d\theta d\psi}\right|_{\psi=0} = 1.327 \times 10^{13} E^2\,[\mathrm{GeV}]\, I[\mathrm{A}]\, H_2(y)$$

with $y = \epsilon/\epsilon_c$.

The vertically integrated distribution gives the horizontal flux density in practical units $[photons/(smrad0.001BW)]$:

$$\left.\frac{d^2F}{d\theta}\right|_{\psi=0} = 2.457 \times 10^{13} E\,[\mathrm{GeV}]\, I[\mathrm{A}]\, G_1(y).$$

The functions H_2 and G_1 are obtained from modified Bessel functions of the second kind, see X-ray data booklet [4].

4.3 Monochromator

Bragg equation:

$$n\lambda = 2d\sin\theta$$

θ is the grazing angle, 2 d is the highest wavelength. Si (111): $2d = 6.27$ Å. The angle is shown on Fig. 9.

4.3.1 Energy Resolution

We start from the Bragg equation with $n = 1$.

$$d\lambda = 2\sin\theta\ \Delta d + 2d\cos\theta\ \Delta\theta$$

and a resolving power:

$$\frac{\lambda}{\Delta\lambda} = \frac{d}{\Delta d} conv \frac{\tan\theta}{\Delta\theta}$$

4.3.2 Asymmetrical cut crystal

The specified asymmetry angle was $\alpha = 0.28°$. We measured $\alpha = 0.172°$.

The symmetry factor b is defined:

$$b = \frac{\sin(\theta_B - \alpha)}{\sin(\theta_B + \alpha)}$$

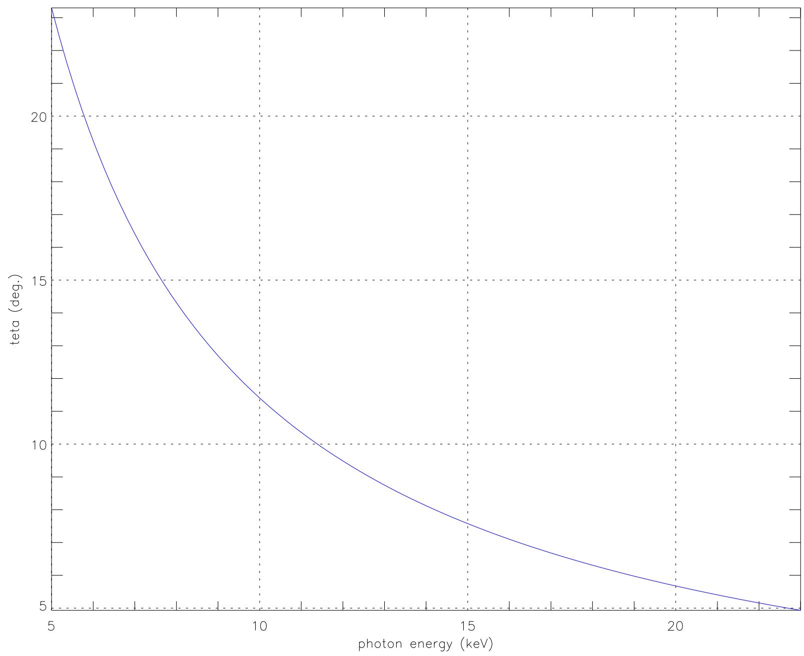

Figure 9: Monochromator angle θ for Si (111).

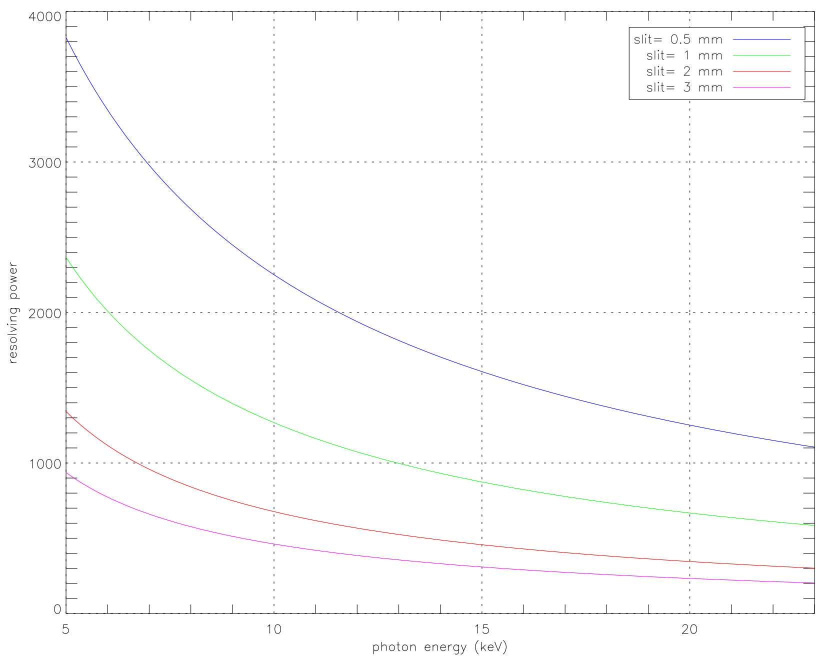

Figure 10: Expected resolving power for different slit settings.

The asymmetric factor scales beam width and divergence. The phase space volume is constant:

$$\omega_1 S_1 = \omega_2 S_2$$

$$S_2 = S_1/b$$

$$\omega_2 = b\omega_1$$

4.4 Mirror

The mirror has a measured short radius of $\rho = 30.8\,\mathrm{mm}$. We measured slope error of $1.6\,\mu\mathrm{rad}$. The position of the mirror is 7.75 m, the nominal grazing angle 4 mrad. The mirror bender has been calibrated with the LTP. We determined the following calibration constants:

$$dx[\mathrm{mm}] = 5.4059 - 0.40772\,R[\mathrm{km}] + e^{-1.2468\,(R[\mathrm{km}] - 3.3215)}$$

and the inverse function:

$$R[\mathrm{km}] = 1.2084 + 0.027026\,dx[\mathrm{mm}] + e^{-0.33289\,(dx[\mathrm{mm}] - 7.4157)}$$

with the shift dx at the bender stage and the mirror radius R.

The sag of the mirror as function of the Radius R can be approximated by:

$$sag = \frac{l^2}{8R}$$

l is the length of the mirror, the result is shown on Fig. 11. The focusing equations for a toroidal mirror are:

$$\frac{1}{s1} + \frac{1}{s2} = \frac{2}{R\,\cos\theta}$$

and

$$\frac{1}{s1} + \frac{1}{s2} = \frac{2\,\cos\theta}{\rho}$$

$s1$ and $s2$ are the source and image distance R the long-, ρ the short radius and θ the angle to the normal of the mirror. A summary is given on Fig. 11. On the figure we used $pitch$ for the grazing angle!

4.4.1 Longitudinal Coherence

The coherence length is given by

$$l_c = \frac{\lambda^2}{2\Delta\lambda}$$

. With the resolving power $R = \lambda/\Delta\lambda$ we receive

$$l_c = R\lambda/2$$

For 10 keV ($\lambda \approx 0.1\mathrm{nm}$), a monochromator with a resolving power of 2000 gives a coherence length of $0.1\mu m$.

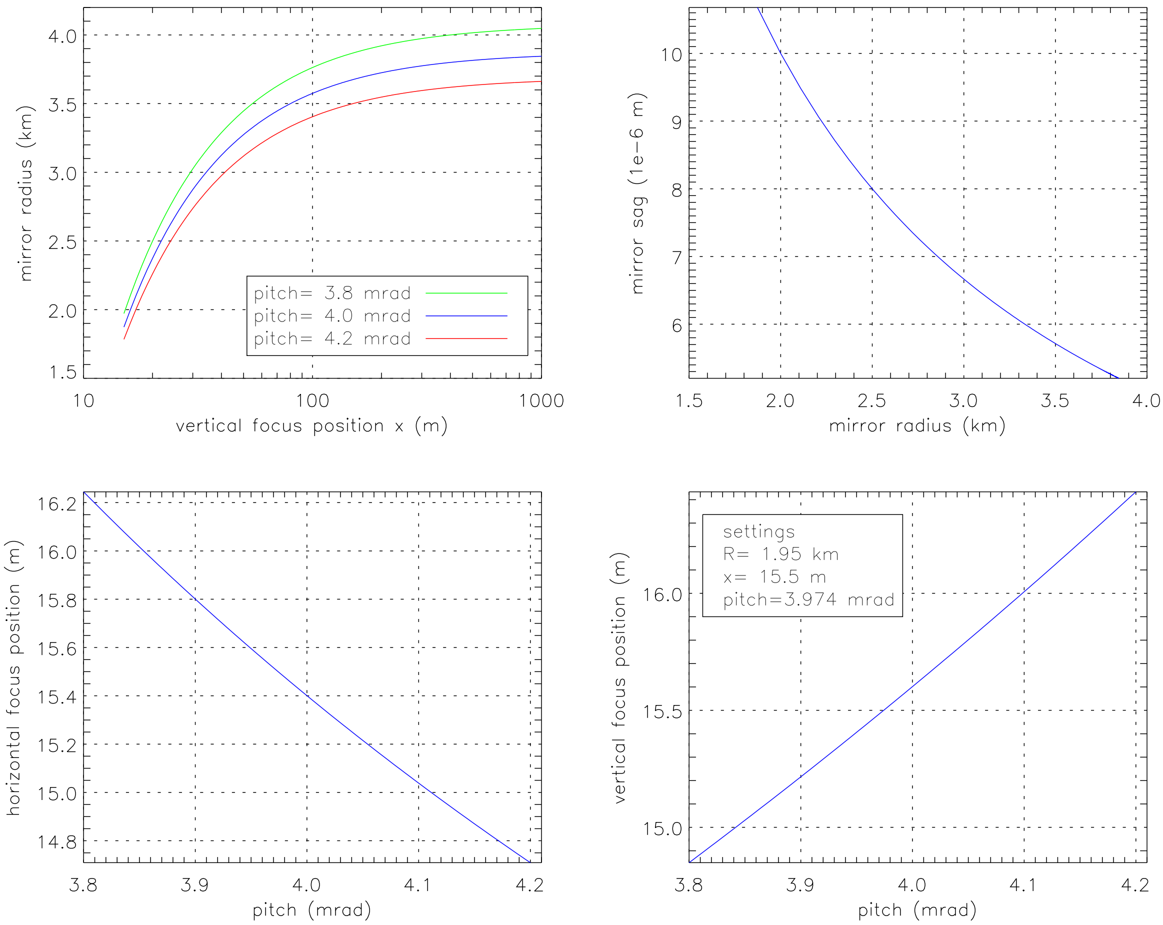

Figure 11: Mirror summary: bender radius, sag and focusing distances as function of the pitch. The vertical focus position is calculated for a given setting of the bender.

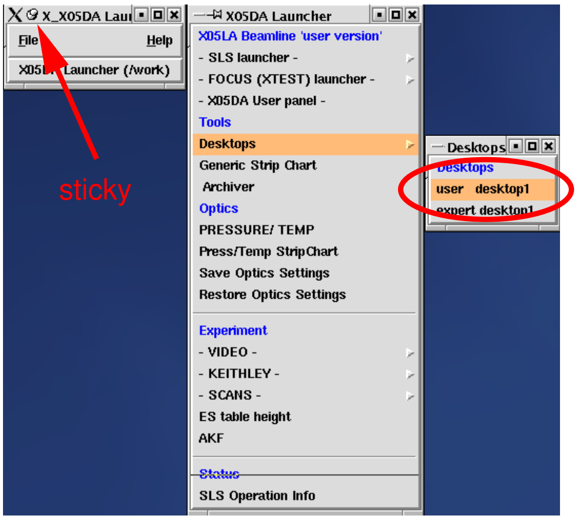

Figure 12: The X_X05DA launcher- start user desktops.

4.4.2 Transverse Coherence

$$d\theta = \frac{\lambda}{2\pi}$$

d is the source width and θ the observation angle, i.e. on the left side we find the emittance of the electron beam.

5 Beamline Operation

5.1 General Remarks

The beamline network is isolated from the rest of the PSI network by a switch. Each user logs in at the beamline console (the 4-head Linux computer in the control room of X05DA) *x05da-cons-1* with his own experiment account name and password. Experiment accounts are generated by the X05DA beamline manager, example for a account name: *e12345*. There is a special account called *x05da* for commissioning by the beamline staff.

The data at the experiment account can be accessed from the users regular account on afs with the command `blmount`.

5.2 Basic Operation

After login the X_X05DA launcher appears. It is recommended to make it ”sticky” (KDE window decorations) and start the default set of applications. *launcher* → *Tools/Desktops* → *user desktop1* as shown on Fig. 12.

The main user panel is shown on Fig. 13. The 3 buttons in the field on the lower left (*control switches and mode selection*) control the basic beamline operation. The very left switch is the main on/off switch. *On* means: it opens the valves and switches on the cooling. It may take a few hours until the crystal temperature is less than -80°C then we reach the standby mode.

If we switch to *off* – the valves, shutters are closed and the cooling is switched off.

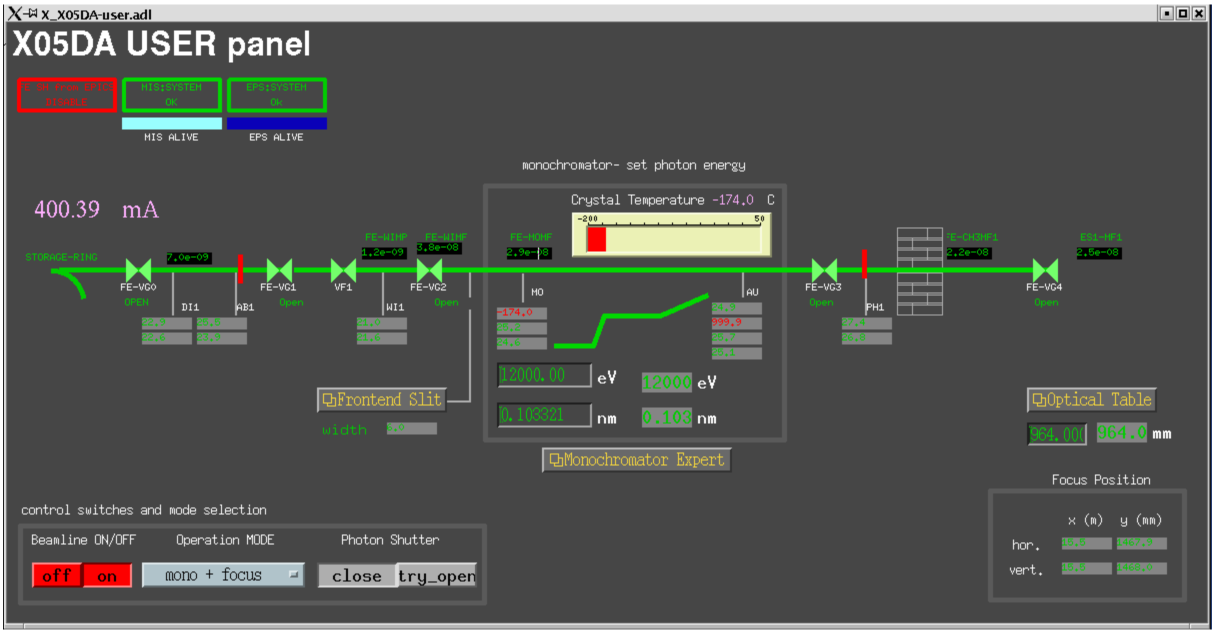

Figure 13: The main user panel.

The pop-up menu *Operation Mode* selects the operation mode of the beamline i.e. whether we use monochromator or/and focusing.

With the right button *Photon Shutter* we switch the light on and off[5]. This requires that the safety search has been done and the hutch has been locked. The first time after the hutch has been accessed the open button at the door of the lead hutch must been pressed once before the on/off function from the panel works.

The panel shows the pressures and temperatures along the beamline, the ring current and allows to set the photon energy and the height of the experimental table. At the right side it shows the calculated focal positions. There are buttons to launch a menu to control the front end aperture and the monochromator expert menu to fine tune the monochromator, the apertures and the focusing mirror. These menus are for experts only!.

The save/restore functionality allows to save and restore an (optimized) parameter set. The ioc based scans are implemented to do 1, 2 or even 3 dimensional scans of any process variables. The scan records scan a number of positioners and record a number of detectors. The result is saved in a mda file which can be processed with the IDL scan library or as an ASCII file by `mdals`.

Analog cameras can be hooked up to a video server. The server provides mpeg4 coded rtp and rtsp streams and jpeg images i.e. one can store jpeg files, monitor and/or record the streams. Default calling sequences are available via the launcher. For special requests the applications are available through the command line and the frame rate etc. can be configured with the web interface.

6 Performance – Expectations and Measurements

6.1 Photon Flux

Photon flux measurements have been done with Si photo diodes from IRD. First we used a 1 cm^2 diode AXUV-100. We did not have a diode with a calibration from PTB etc.– we used the efficiency curve from the vendor

[5]This involves the operation of the photon shutter and absorber in the right sequence.

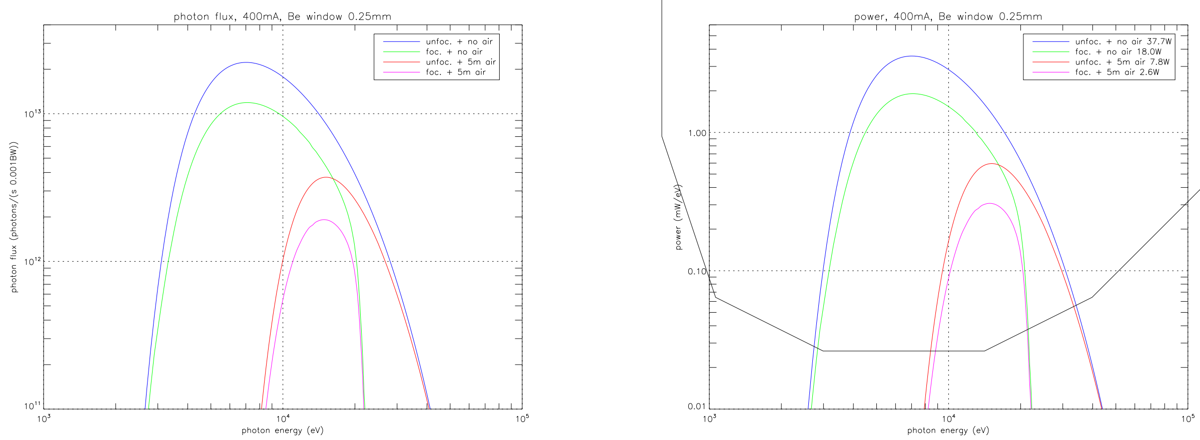

Figure 14: Photon flux and power for focused and unfocused pink beam, with/without 5 m air path.

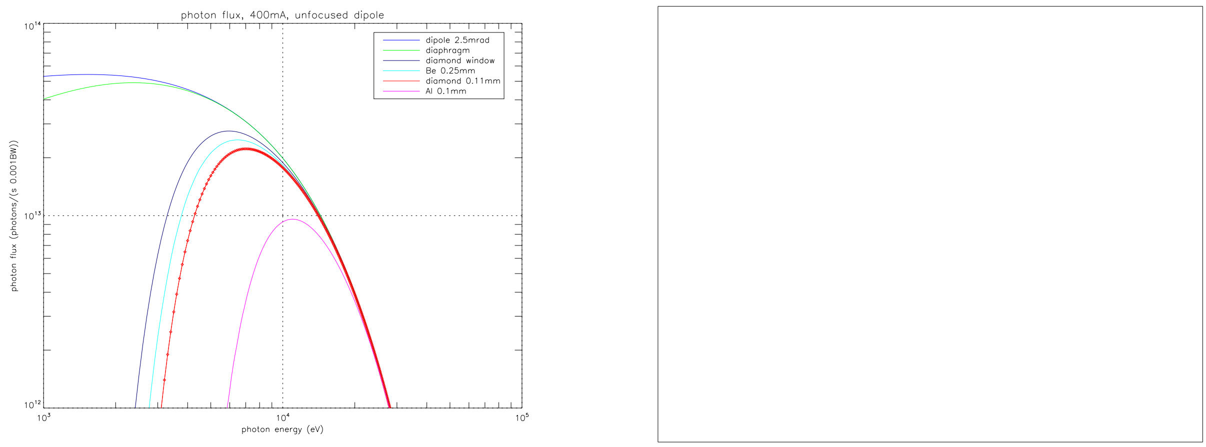

Figure 15: Photon flux and power for unfocused pink beam, different window materials.

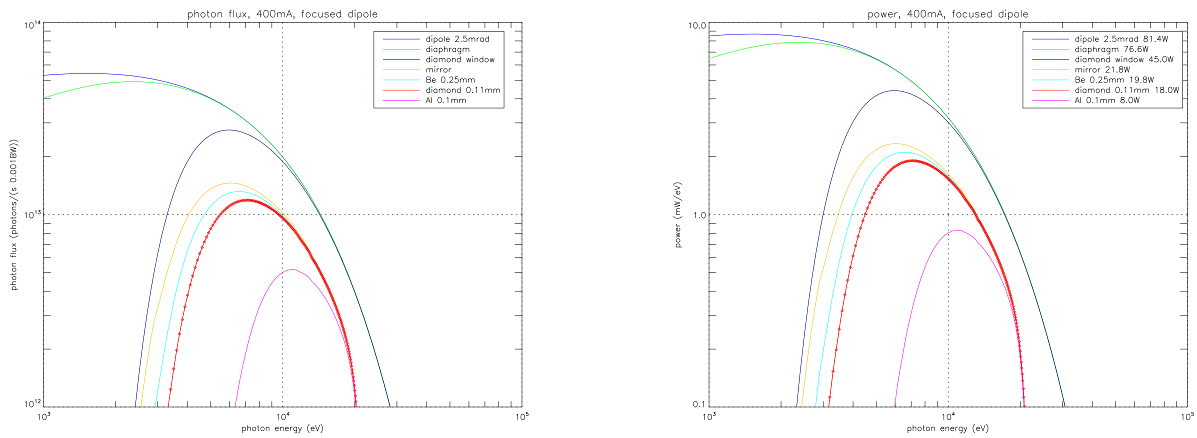

Figure 16: Photon flux and power for focused pink beam, different window materials.

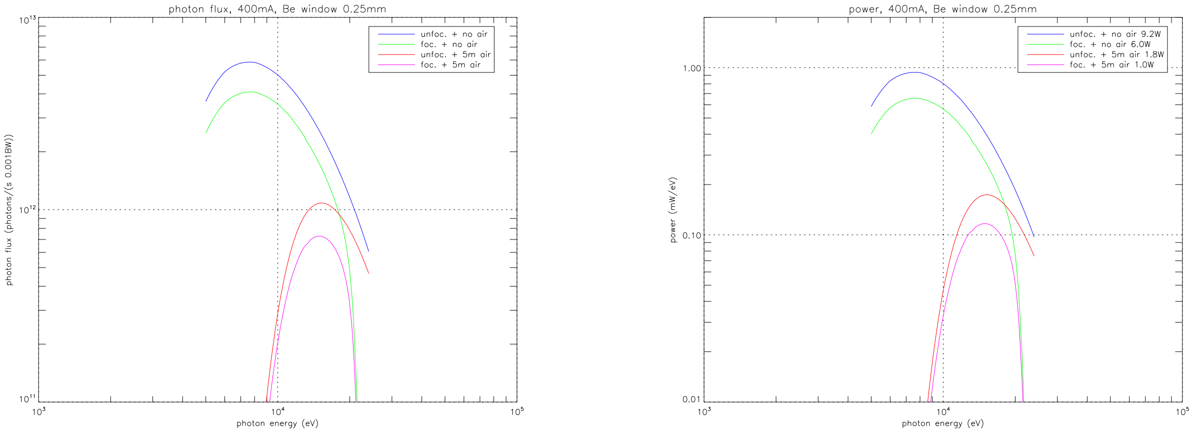

Figure 17: Photon flux and power for focused and unfocused monochromatic beam, with/without 5 m air path.

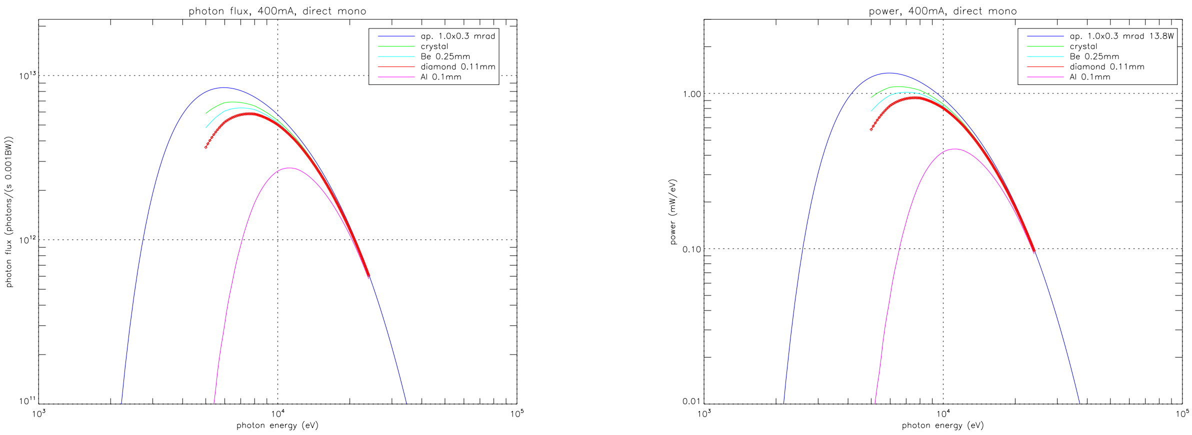

Figure 18: Photon flux and power for unfocused monochromatic beam, different window materials.

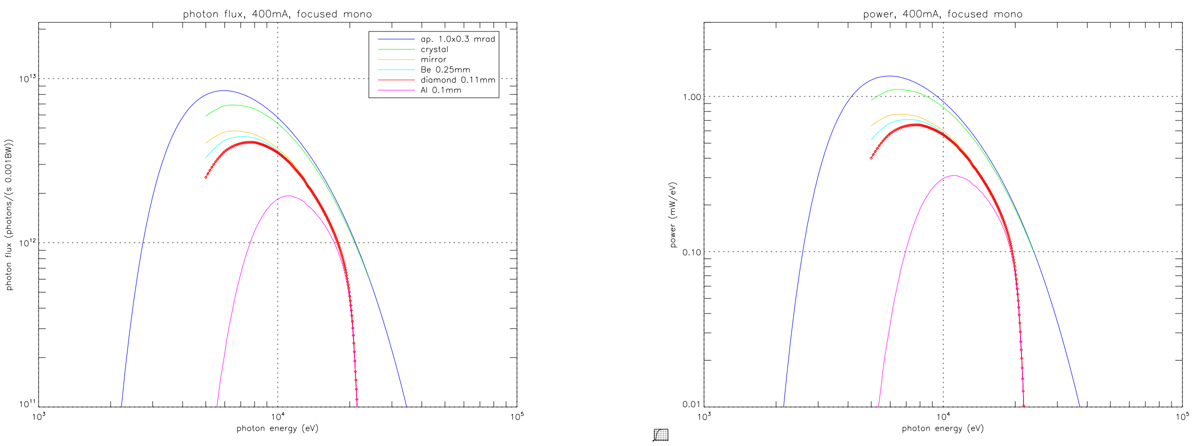

Figure 19: Photon flux and power for focused monochromatic beam, different window materials.

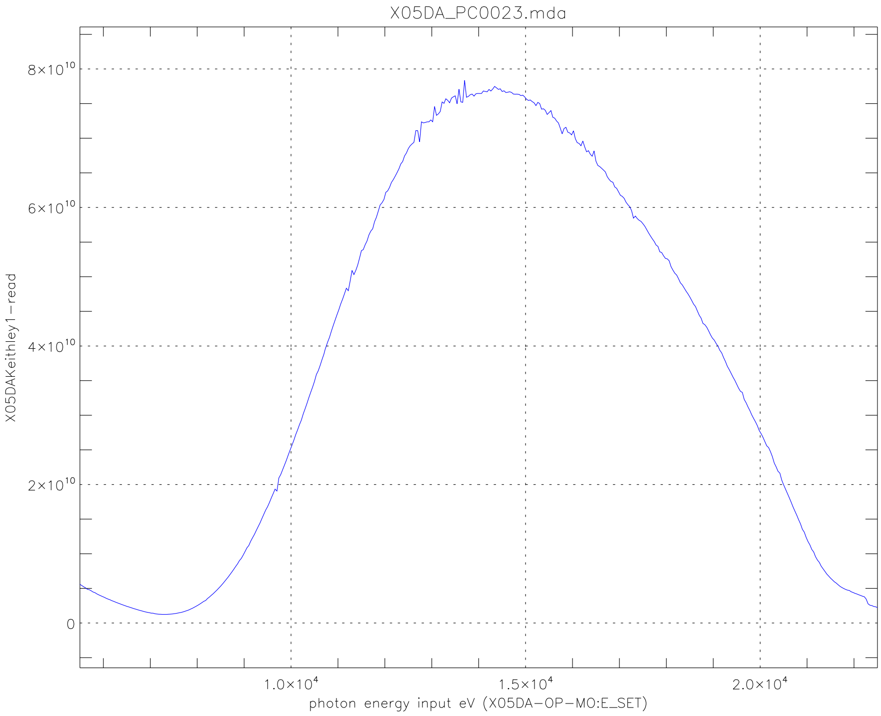

Figure 20: Measured photon flux. Measurement from June 2007 with Be window and 5 m air path. Units: photons/(s ΔE).

which goes up to 6 keV. For higher energies the transmission has to be taken into account which depends on the thickness. Maik Kaiser determined a thickness of 224 μm for our diode[6]. The absolute accuracy we reached with this procedure is not very good. We estimate an error of $\pm 30\%$. We observe also significant differences to measurements with diodes from Hamamatsu. The accuracy shall be improved with the AXUV-20HE1 we got recently. These diodes are optimized for high energy applications and have a known thickness. The efficiency normalization is available in our standard IDL data treatment library.

The photon flux and power density predictions are shown on Fig. 14 to 19. The curves show the flux/power after a certain optical element. Calculations are given for monochromatic and pink beam mode, for focused and unfocused mode and for various materials of the final vacuum window. The red curve with symbols shows the actual situation with the 100 μm thick diamond vacuum window which will be installed in November 2007. The "with air" curves simulate the 5 m air path i.e. if the pipe between the diamond window and the experiment is vented. If applicable the integrated power is shown as well.

Fig. 20 shows the flux measurement from June 2007 with Be window and 5 m air path using the efficiency curve from IRD and assuming 224 μm thickness.

6.2 Higher Order Contamination

The higher order contamination can be estimated by the flux measurements shown on Fig. 21. We measured the photon flux with the AXUV Si- photo diode with 5 m air path and subsequently adding 0.5 mm thick Al plates in air path. We can model the flux with XOP. From the model we expect a steady increase of the flux up to about 15 keV. In our measurements we saw some intensity also at low energies which can be explained as higher orders.

[6] He measured the flux while rotating the diode.

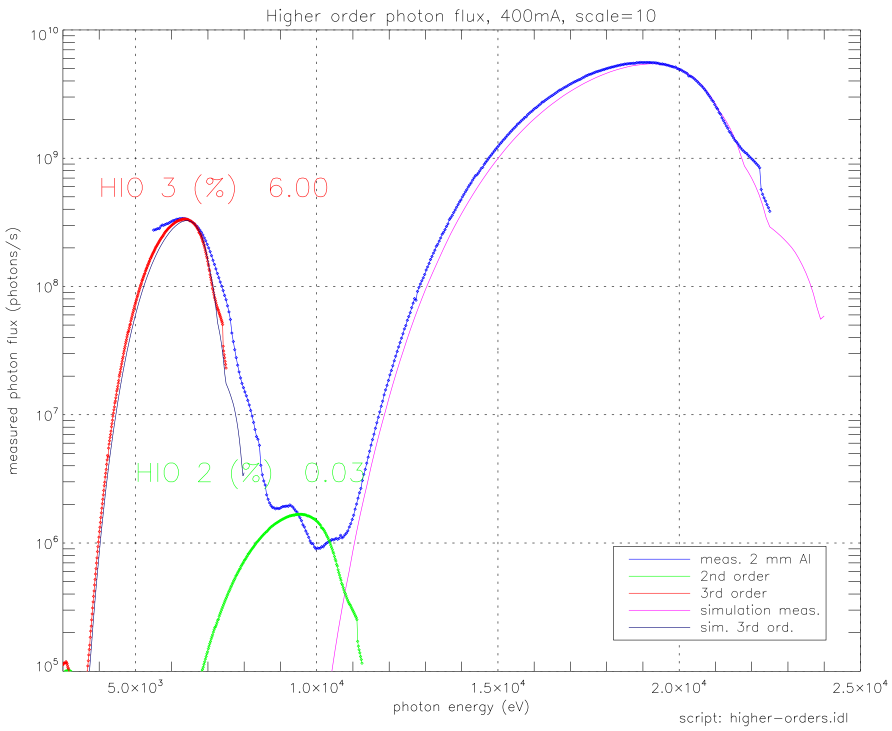

Figure 21: Higher order contamination.

We measured 6% third order and 0.06% second order at E/n with the photon energy E and the order n. Attention — the 100% level is taken at the energy E. Usually one wants to know the higher order contamination at an energy E, for this a renormalization has to be applied.

6.3 Focus

6.3.1 Spot size measurements

Focus measurements have been done with a scintillator crystal and a microscope with a CCD camera. Between scintillator and objective we put a plane mirror in 45°, so that the microscope could be installed transverse to the beam to avoid any radiation damage. The zoom and focus of the microscope could be remote controlled. The images have been red out with a VME- frame grabber. Data evaluation has been done with IDL. We applied a 2-dimensional Gaussian fit, determined center and width and updated the appropriate EPICS channels. Alternatively we used 1-dimensional fits on the projections. We used a Sony XC-55 camera in progressive scan mode. The illumination time can be controlled from $1 \ldots 250\,\mathrm{ms}$. Usually we did the measurements with fixed gain. The camera allows also manual gain and automatic gain. The video's have been taken with automatic gain and PAL mode.

Fig. 22 shows the focus at 16.5 m with a photon energy of 12 keV (focused monochromatic mode). The result of $(70\mathrm{v} \times 140\mathrm{h})\,\mu\mathrm{m}$ FWHM is in good agreement with the ray tracing calculation shown on Fig. 24.

Fig. 23 shows a sequence of images at 16.5 m while changing the mirror radius and nominal focus position respectively. We found the optimum focus at a nominal focus position of 16.8 m. The small difference of about 30 cm indicates our radius calibration at the LTP was already very good. The corresponding spot size measurements are shown on Fig. 25. The FWHM width of in the horizontal and vertical direction are shown as function of the

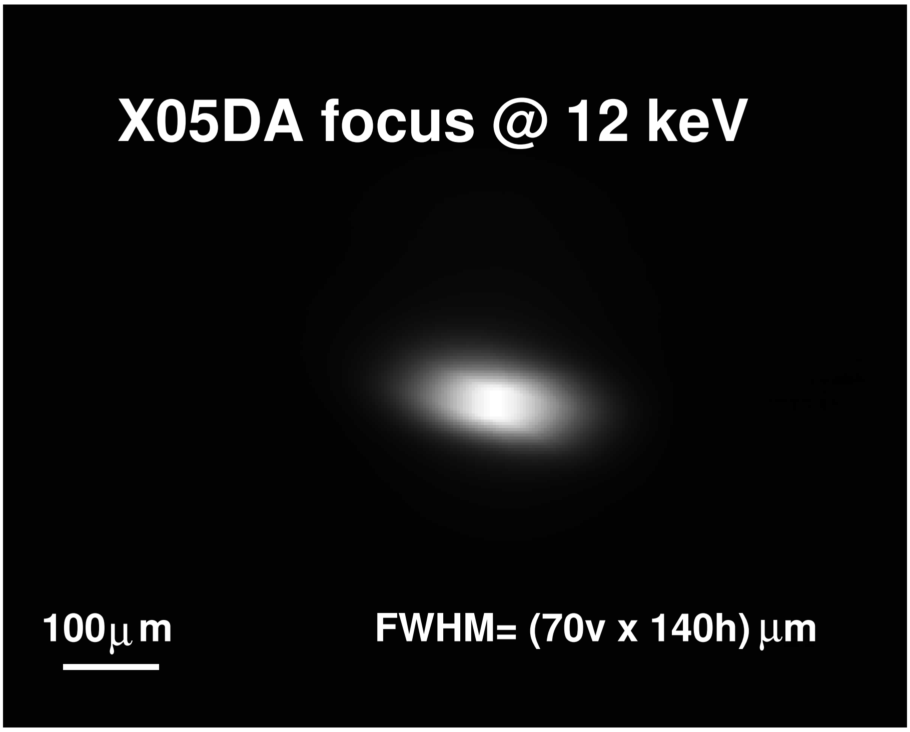

Figure 22: X05DA monochromatic focus at 12 keV.

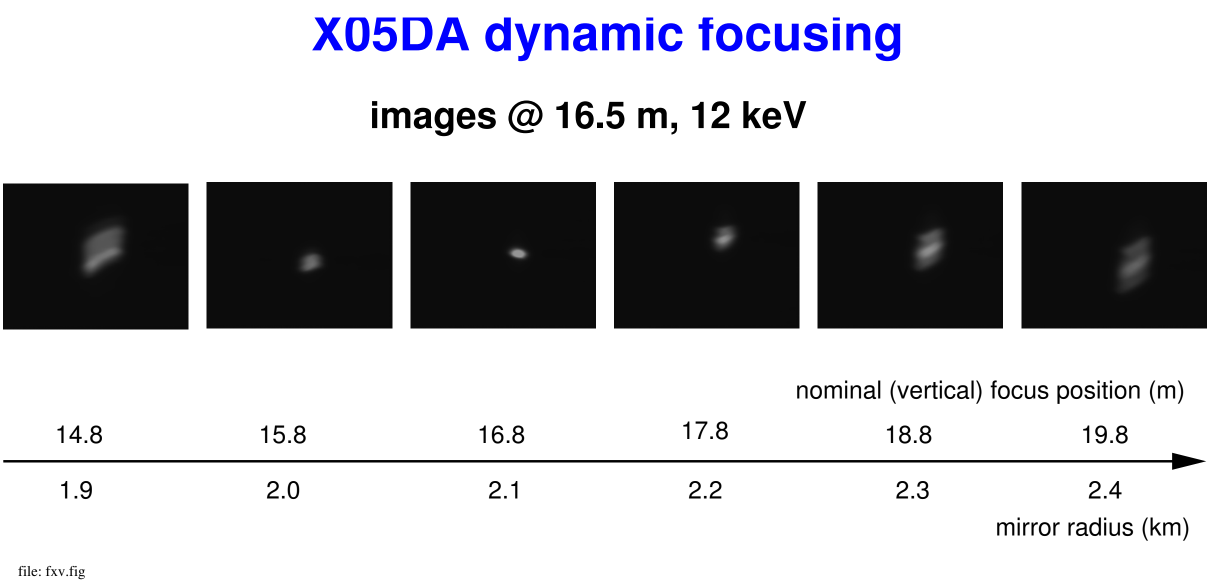

Figure 23: Spot shape while changing the radius of the mirror.

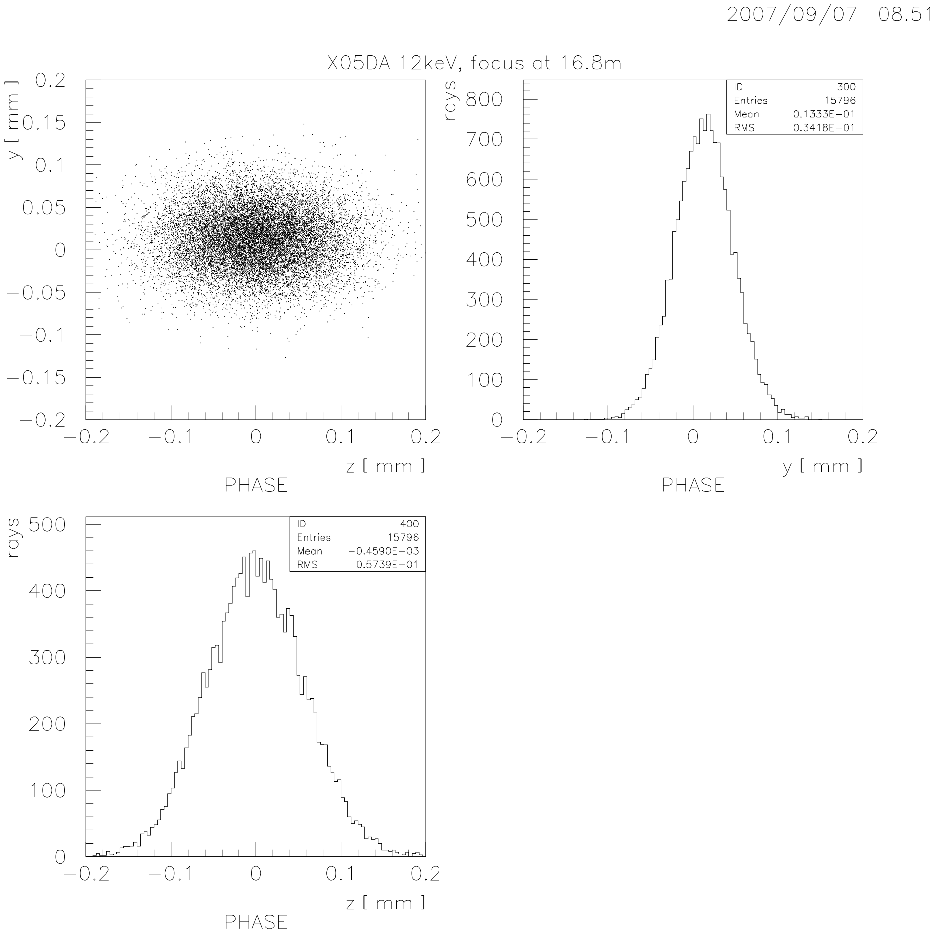

Figure 24: Ray tracing calculation of the focus at 12 keV.

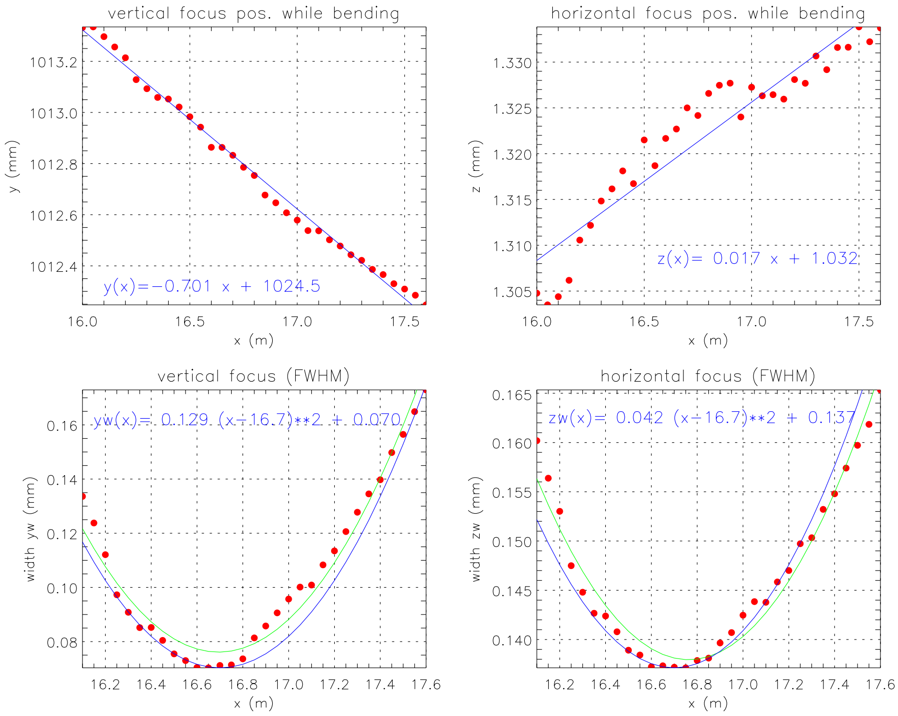

Figure 25: Measured spot size as function of the nominal focus position (mirror radius) and fit.

nominal focus position, i.e. as function of the bending radius of the focusing mirror. The fit parameter are given in the plot. Fig. 26 shows the measurements and the extrapolation by using the fit.

Fig. 27 shows the measured focus dependence as function of the pitch. Fig. 28 the extrapolation. With the fit we determined $\frac{dy}{d\theta} = 17.445$ from our geometry we expected 17.438 i.e. the relative difference is only $4\ 10^{-4}$.

Fig. 29 shows the focus as function of the mirror height. Fig. 30 the focus as function of the photon energy. The $10\,\mu\mathrm{m}$ step at about 17 keV comes from Y in the scintillator crystal. We verified this by measurements with another type of phosphor.

We measured the focused pink beam- the size was: $(94\mathrm{v} \times 148\mathrm{h})\mu\mathrm{m}$ at a front end opening of 15 mm and 1 cm Al. Taking these numbers for a simple approximation — the spot size is $0.014\,\mathrm{mm}^2$ with 58% of the intensity[7]. From Fig. 14 or 16 we expect 18 W after the last window for focused pink beam. This means 10.4 W are inside FWHM and we end up with a remarkable power density of about $750\,\mathrm{W/mm}^2$ averaged over FWHM and $1.5\,\mathrm{kW/mm}^2$ at maximum.

6.3.2 Dynamics (Movies)

We took some videos which demonstrate the change in focus shape dependence on other parameters. We also see the vibrations and damping when we move motors. The movies are summarized in Tab. 1[8].

[7] Assuming a Gaussian distribution 76% of the intensity are inside FWHM, if we take two distributions we end up with: $0.76^2 = 0.58$.
[8] The files can be viewed for instance with mplayer.

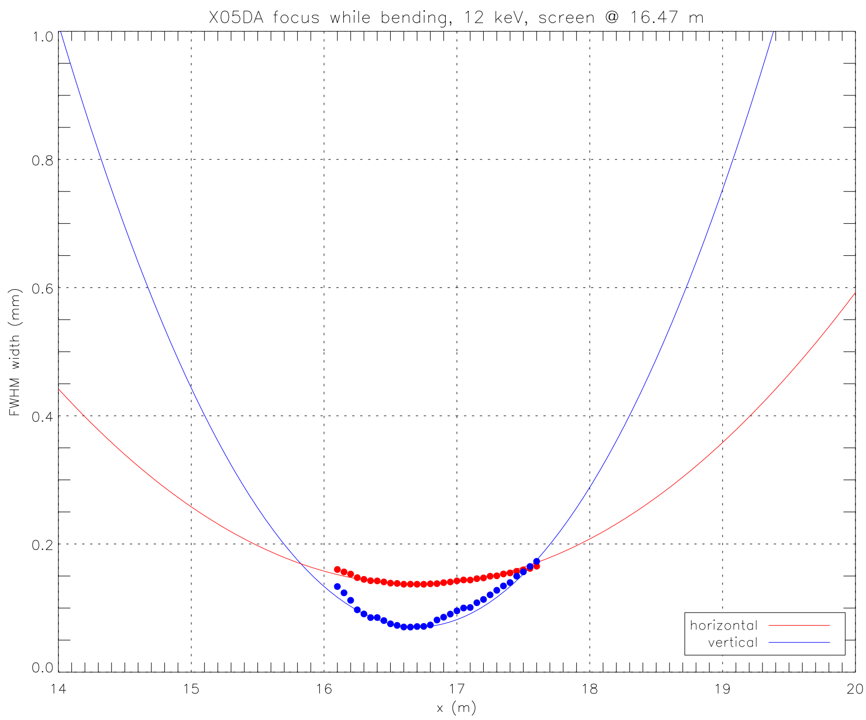

Figure 26: Measured spot size as function of the nominal focus position (mirror radius) and extrapolation.

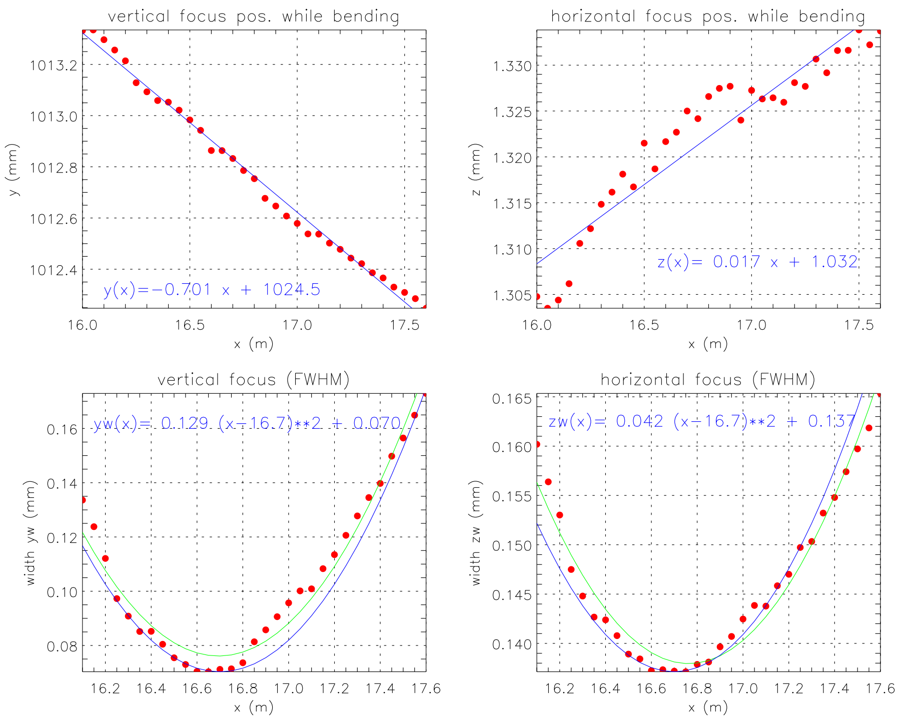

Figure 27: Measured spot size as function of the pitch and fit.

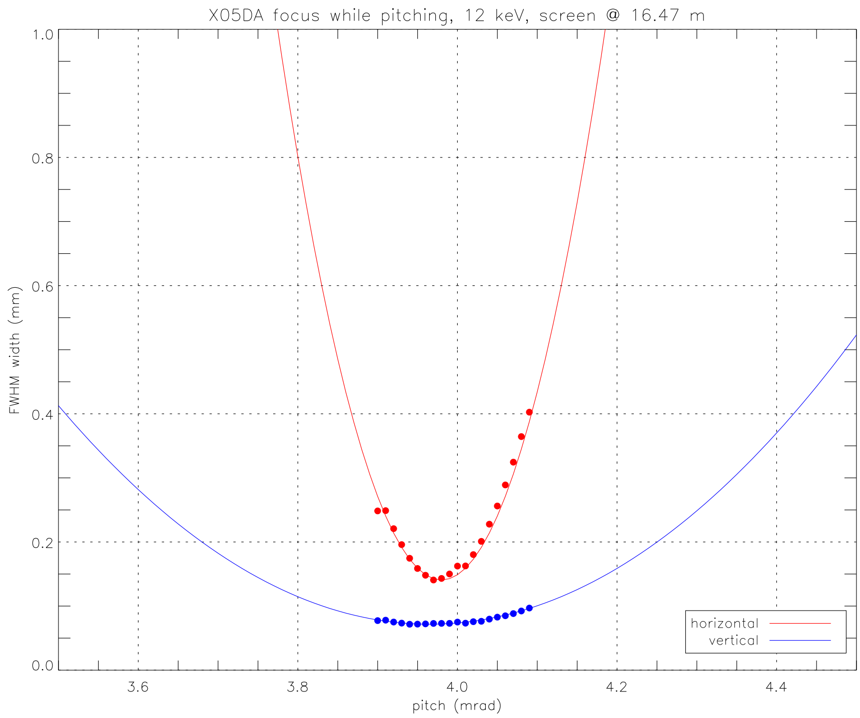

Figure 28: Measured spot size as function of the pitch and extrapolation with the fit.

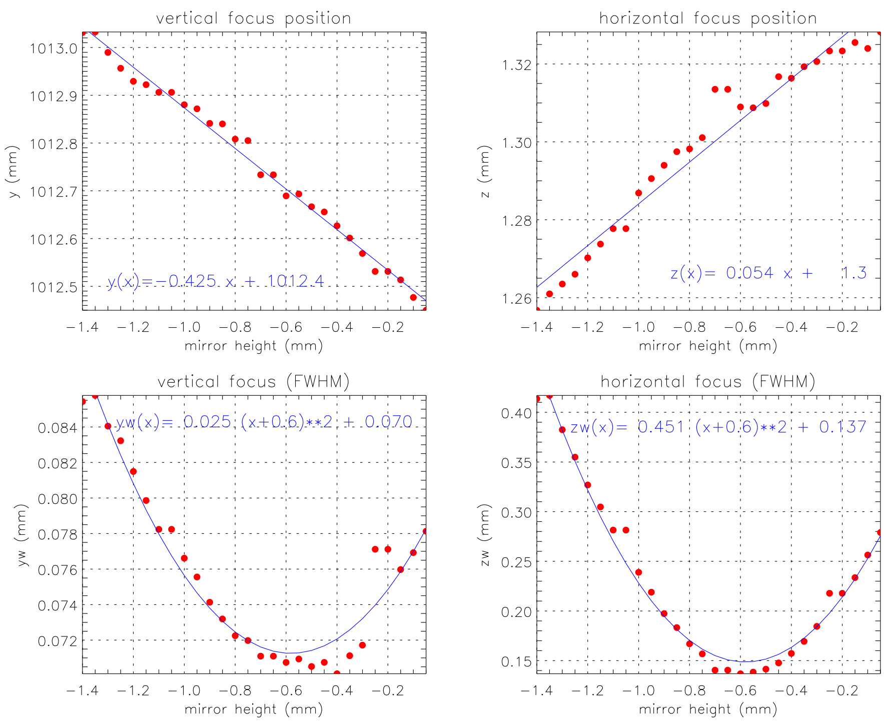

Figure 29: Measured spot size as function of the mirror height and fit.

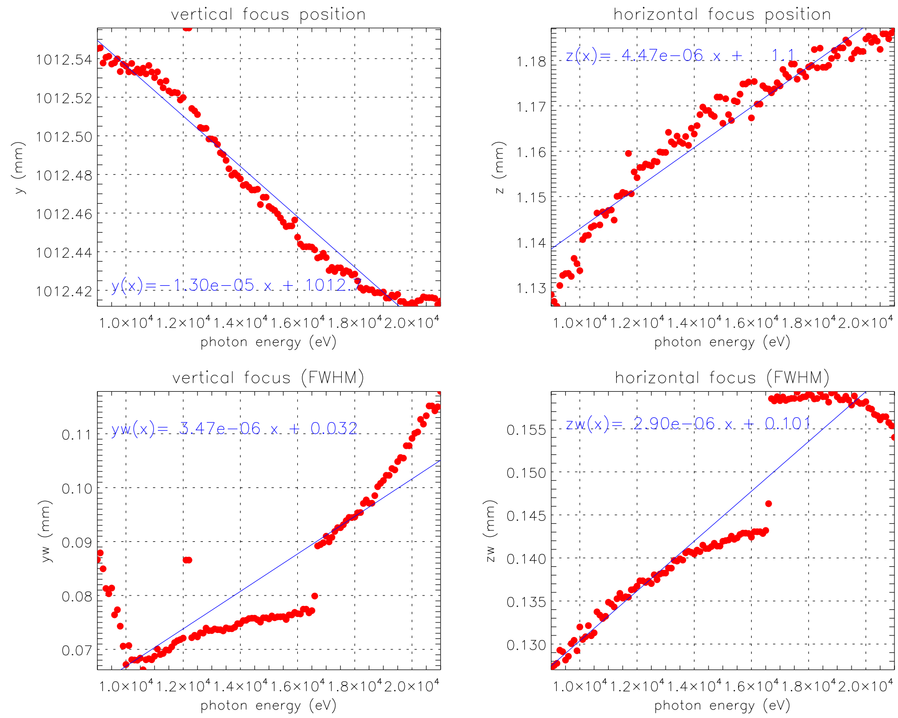

Figure 30: Measured spot size as function of the photon energy and fit.

Table 1: Movies of focus dynamics.

movement	description	file
no	Focused monochromatic beam. We see small vibrations- the source could not be determined so far.	default.avi
yaw	$0.374 \rightarrow 0.274 \rightarrow 0.474 \rightarrow 0.374$ step: 0.01	yaw.avi
FXV	$16.7 \rightarrow 16.1 \rightarrow 17.1 \rightarrow 16.7$	fxv.avi
pitch	$0.397 \rightarrow 0.3965 \rightarrow 0.3975 \rightarrow 0.397$	pitch.avi
height	$-0.6 \rightarrow -1.2 \rightarrow -0.3 \rightarrow -0.6$	height.avi
trz	$-14.7 \rightarrow -15 \rightarrow -14 \rightarrow -14.7$	trz.avi
AU vpos	$2 \rightarrow out \rightarrow 3 \rightarrow 2 \rightarrow 1 \rightarrow 0.5 \rightarrow 2$	au-vpos.avi
FE width	$6 \rightarrow 10 \rightarrow 6 \rightarrow 0 \rightarrow 6$	fwidth.avi
energy	$12 \rightarrow 16 \rightarrow 12$, lock2dy: on	e.avi
energy	$12 \rightarrow 16 \rightarrow 12$, lock2dy: off	elockoff.avi
energy	$10 \rightarrow 20$	e10-20.avi

6.4 Energy resolution and resolving power

The resolving power has been checked with a Cu foil in transmission at about 8 keV. The measurements have to be repeated after the installation of the new diamond window[9].

7 Status and Outlook (Oct 2007)

The installation of the diamond vacuum window and the following vacuum pipe is scheduled for Oct 2007. With the pipe the beamline can be used for reasonable measurements. The following characterization measurements are planned afterward:

- photon flux in focused and unfocused monochromatic mode
- power measurement in focused and unfocused pink beam mode
- resolving power at selected energies

8 History

- 1998/ 1999 optics beamline — nice to have UF, RA
- summer 2002 check feasibility of optics beamline at BM X05DA UF, RA, FvdV.
- March 2003 proposal to ETH- Rat (reserve money).
- Spring 2003 UF presented the ideas at the SLS quo vadis meeting in Wettingen.
- Summer 2003 front end delivered and tested.
- September 2003 financing ensured (550 kCHF for an optics lab consisting of a clean room with Long Trace Profiler (LTP) 200 kCHF and a beamline 350 kCHF.
- September 2003, new concept- adopt ALS concept with optics inside the tunnel.
- October 2003, we may have the drawings of ALS beamline 11.3.1, received OK from H. Padmore
- October 31, 2003, meeting with S. Zelenika, PSI starts the development of a braced CVD diamond window for the X05DA beamline.
- November 24, 2003 reply from ETH- Rat– (no reserve money available), decision RA to proceed with the beamline as part ot the optics lab (budget).
- June 2004, discussion with Howard Padmore at SLS.
- October 2004, start detailed mechanical design at PSI.
- September 2005, start manufacturing with monochromator at PSI.
- Januar 2006, design finished.
- May 2006, monochromator – mirror assembly delivered to SLS.
- May 2006, poster presentation at SRI 2006 in Daegu, Korea.

[9]With the air path no almost flux was left at 8 keV– see flux simulations.

- June 2006, mirror delivered, successful mirror bonding.
- September 5, 2006 installation inside the tunnel.
- October 2006 first light in the monochromator and some days later in the experimental hutch.
- September 2007, commissioning results available, flux, focus, higher orders etc.
- November 2007, decision: replace Be window with diamond window, vacuum pipe instead of 5 m air path.
- April 2008, patch panel for 32 motors, 16 encoders, 8 temperatures etc. in operation

References

[1] Flechsig, U., Abela, R., Betemps, R., Blumer, H., Frank, K., Jaggi, A., MacDowell, A. A., Padmore, H. A., Schönherr, V., Ulrich, J., Walther, H., Zelenika, S., and Zumbach, C., "The SLS Optics Beamline," in *Synchrotron Radiation Instrumentation: 9th Int. Conf.*, edited by J.-Y. Choi and S. Rah, AIP, Mellville, New York, 2007, vol. 879 of *AIP Conference Proceedings*, p. 890.

[2] Padmore, H. A., Thompson, A., and Jun, F., "A double crystal monochromator using tangentially bent crystal in combination with toroidal mirror focusing" , *Nucl. Instr. Meth. Phys. Res. A*, **467**, 650–653 (2001).

[3] Thompson, A. C., Padmore, H. A., Oliver, A. G., Teat, S. J., Celestre, R. S., Clark, S. M., Domning, E. E., Franck, K. D., and Morrison, G. Y., "A Simple High Performance Beamline for Small Molecule Chemical Crystallography," in *Synchrotron Radiation Instrumentation: 8th Int. Conf.*, edited by T. Warwick, J. Artur, H. Padmore, and J. Stöhr, AIP, Mellville, New York, 2004, vol. 705 of *AIP Conference Proceedings*, pp. 482–485.

[4] Thompson, A., et al., X-ray data booklet (2001), URL http://xdb.lbl.gov.